A Three-port Dual Active Bridge Resonant Based with DC/AC Output

Mohammad Nilian
Department of Electrical and
Computer Engineering
University of Central Florida
Orlando, FL, USA
mohammad.nilian@ucf.edu

Reza Rezaii

Department of Electrical and

Computer Engineering

University of Central Florida

Orlando, FL, USA

reza.rezaii@ucf.edu

Md Safayatullah Electric Drive System Ford Motor Company Dearborn, MI, USA msafayat@ford.com Sahin Gullu

Department of Electrical and

Computer Engineering

University of Central Florida

Orlando, FL, USA

sahin.gullu@ucf.edu

Fahad Alaql
Department of Electrical Engineering
Imam Mohammad Ibn Saud Islamic University
Riyadh, Saudi Arabia
faaql@imamu.edu.sa

Issa Batarseh

Department of Electrical and Computer Engineering

University of Central Florida

Orlando, FL, USA

issa.batarseh@ucf.edu

Abstract—This paper introduces a three-port dc-dc-dc/ac converter based on dual active bridge resonant (DABR) topology that can integrate two dc input sources such as photovoltaic (PV) panels and provide one dc/ac output (battery/grid). The proposed converter is well-suited for grid-tied photovoltaic and energy storage systems. The power flow occurs due to the phase-shift between the primary and secondary switches. We employ triple phase-shift (TPS) modulation that confirms zero-voltage-switching (ZVS) of all the switches for a wide range of output voltage and thereby, increases the overall efficiency. The operating principles of the three-port converter have been described. Both simulation and experimental results demonstrated in the paper validate the feasibility of the proposed converter.

Keywords—dual active bridge, electric vehicle, grid, resonant converter, soft switching, three-port converter, zero-voltage switching.

I. INTRODUCTION

With the goal of reducing fossil fuel related CO₂ emission, the integration of PV system into the power grids is increasing swiftly. In 2022 U.S. has installed 18.6 GW of solar PV capacity [1]. Additionally, residential and utility-scale PV system price (\$/W) has been declining over the past few years. However, high penetration of PV into grid still faces significant challenges due to lack of innovative power electronic systems [2]. Research and development of multiport converters are essential because they inherit a smaller number of power stages which results in high efficiency, high power density, high reliability, and low cost [3]-[6].

There are two categories of multiport converters such as isolated and non-isolated converters. Isolated converters provide galvanic isolation which enhances the safety of the system. There are a few isolated converter topologies such as LLC

resonant converter, dual active bridge converter, AC-link universal converter, and phase shifted full bridge converter [7].

The multiport PV input LLC converter has been proposed in [4] and [8] by connecting each PV source to one half-bridge configuration. Using the common resonant tank reduces the cost and increases the power density of the converter. The LLC resonant converter utilizes frequency modulation which adds complexities in reverse operation. The phase shifted full bridge converter has secondary side diodes that generate more power losses and do not allow reverse power flow.

Dual active bridge resonant (DABR) topology is appropriate for the dc-dc stage or dc-ac stage due to its high-power density, high efficiency, bidirectionality, isolation, soft switching, and wide voltage transfer ratio [9], [10]. The dc output of DABR is used for connecting to the battery for different applications and can charge or discharge the battery based on the control method [11]. In [12] and [13], a reduced and improved three-port topology is proposed which utilizes DAB based DC-AC topology. Also, an output filter is placed to generate smooth sinusoidal output current.

Traditional dual active bridge converters provide trapezoidal shaped transformer current which possess higher order harmonics and conduction loss is increased [14]. Due to the inclusion of the resonant tank, the current through the transformer is sinusoidal, and therefore, the conduction loss is lower if compared with traditional dual active bridge converter [15]. In addition, the DABR converter provides extended soft switching range due to the adoption of resonant tank. Switching modulations are mainly single-phase shift (SPS), dual phase shift (DPS), and triple phase shift (TPS). SPS causes high switching and conduction loss in light load conditions. DPS extends the ZVS range; however, all the switches cannot achieve

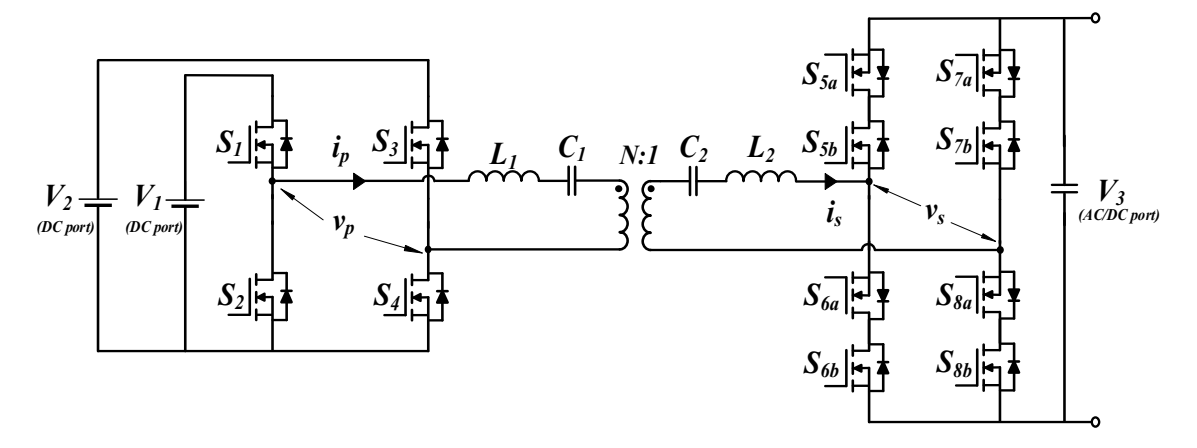


Fig. 1. Circuit schematic of the proposed three-port dc-dc-dc/ac converter based on dual active bridge (DAB) resonant topology.

ZVS. TPS secures ZVS of all the switches even at no-load condition.

In this paper, we propose a three-port converter that integrates two dc input sources with dc/ac output port and can be applicable for microgrid, PV, and electric vehicle (EV) charging applications as shown in Fig. 1. The operating principles of the proposed three-port converter are discussed in Section II. Simulation and experimental results of the converter are demonstrated in Section III. Finally, concluding remarks are drawn in Section IV.

II. OPERATING PRINCIPLE

The circuit operates as a dual active bridge converter between port-1 to port-3 and port-2 to port-3. Due to the inclusion of the resonant tank, the current becomes sinusoidal and conduction loss is reduced. The operating switching waveforms of the converter with dc output have been illustrated in Fig. 2. The power flow between the ports is governed by the three-phase shifts generated by TPS modulation. Three-level voltage waveforms are generated at the primary and secondary side. The current through the resonant tank is sinusoidal. The phase shifts are calculated based on the zero-voltage switching (ZVS) turn on conditions of all switches. The ZVS turn on conditions of all switches can be found by checking the current polarity of the resonant tank during turn on of each switch. The equivalent circuit of this mode can be analyzed with fundamental component analysis. The voltage waveforms shown in Fig. 2 can be represented by their fundamental component. Fourier series representation of any signal $x(\tau)$ is,

$$x(\tau) = \sum_{n=-\infty}^{n=\infty} a_n \, e^{jn\omega_S \tau} \tag{1}$$

$$a_n = \frac{1}{T_s} \int_{t-T_s}^t x(\tau) \ e^{-jn\omega_s \tau} \ d\tau \tag{2}$$

where, a_n is the Fourier series coefficient, T_s is the switching period and $\omega_s = 2\pi/T_s$. Putting n = 1, we can get a_1 which is required to determine the fundamental component of $v_p(t)$ and $v_s(t)$ [16].

$$a_{1,v_p} = V_p \left(\frac{\sin D_1}{\pi} + j \frac{-1 + \cos D_1}{\pi} \right)$$
 (3)

$$a_{1,v_s} = V_s \left(\frac{sin(\delta + D_2) - sin\delta}{\pi} + j \frac{cos(\delta + D_2) - cos\delta}{\pi} \right) \tag{4}$$

The equations of voltage, $v_p(t)$ and $v_s(t)$ are determined as follows,

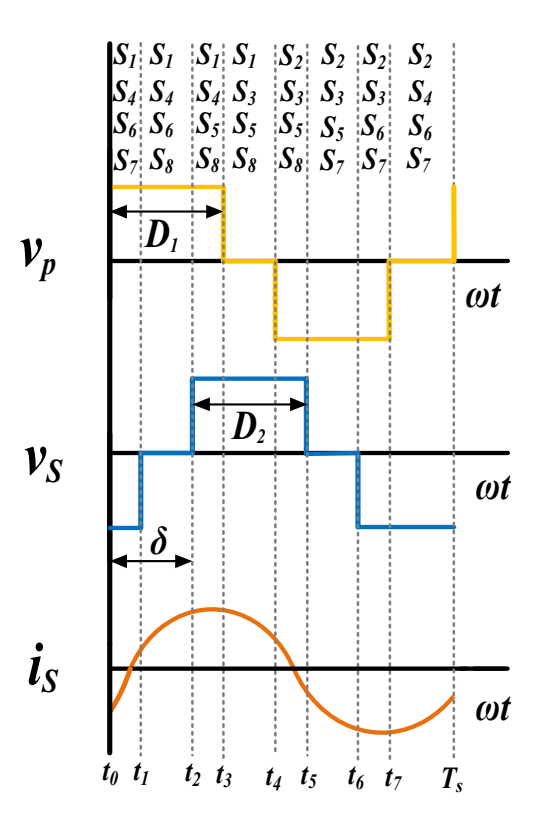


Fig. 2. DABR switching waveforms.

$$v_p(t) = \frac{4V'_p}{\pi} \sin \frac{D_1}{2} \cos \left(\omega_s t - \frac{D_1}{2}\right) \tag{5}$$

$$v_s(t) = \frac{4V_s}{\pi} \sin \frac{D_2}{2} \cos \left(\omega_s t - \delta - \frac{D_2}{2} \right)$$
 (6)

where, V_p and V_s are the peak values of v_p and v_s respectively. The current in the resonant tank, i_s is,

$$\begin{split} i_s(t) &= \frac{4V_p}{\pi\left(\omega_s L - \frac{1}{\omega_s C}\right)} \left[\sin\frac{D_1}{2} \sin\left(\omega_s t - \frac{D_1}{2}\right) - \\ M \sin\frac{D_2}{2} \sin\left(\omega_s t - \delta - \frac{D_2}{2}\right) \right] \end{split} \tag{7}$$

The average output power, P_o and output current, I_o are given as follows,

$$P_{o} = \frac{8 V_{p}^{2} M \sin \frac{D_{1}}{2} \sin \frac{D_{2}}{2} \sin \delta}{\pi^{2} (\omega_{s} L - \frac{1}{\omega_{s} C})}$$
(8)

$$I_{o} = \frac{P_{o}}{V_{s}} = \frac{8 V_{p} \sin \frac{D_{1}}{2} \sin \frac{D_{2}}{2} \sin \delta}{\pi^{2} (\omega_{s} L - \frac{1}{\omega_{s} C})}$$
(9)

where, $M=V_s/V_p$, $V_p=NV_p$, $i_s=Ni_p$, $L=L_1+L_2$, and $C=\frac{c_1c_2}{c_1+c_2}$. To ensure ZVS turn on of the switches, associated parasitic capacitors must be discharged and body diodes should be conducting prior to turn on signals appear at the gate terminals.

The utilization of the back-to-back switches is applied to prevent the secondary bridge from short-circuiting through the anti-parallel diodes of the active switches. Also, the secondary bridge works the same as a cycloconverter. This DABR converter use a high-frequency AC (HFAC) link, generated by either the primary or secondary bridges, to produce a low-frequency AC square wave. This square wave can then be filtered through a low pass filter to produce an AC sine wave. By precisely regulating the PWM on the primary side, the bridge is capable of generating a continuous HFAC output. Consequently, the suggested HFAC link configuration can convert DC input into an AC sine wave, leveraging the transformer's leakage inductance as the AC link [13].

The gate-source pulses of the input bridge are denoted as V_{gs} , as shown in Fig. 3. However, the synthesis of the SPWM on the primary bridge involves alternating the V_{gs} PWM between switches S_1 , S_4 , and S_2 , S_3 . The first-order low pass filter is applied to the output current to generate a sine wave. During the positive half cycle of the 60Hz AC waveform, switches S_5 to S_8 in the output bridges remain activated while the other switches are modulated. Similarly, during the negative half cycle, switches $S_{5,b}$ to $S_{8,b}$ are kept on while the other switches are modulated in a similar manner. This arrangement facilitates the unfolding of the 60Hz AC waveform [13].

The modulation scheme depicted in Fig. 3 maintains a constant phase-shift between the primary and secondary bridges while applying a SPWM pattern on the primary bridge. This approach

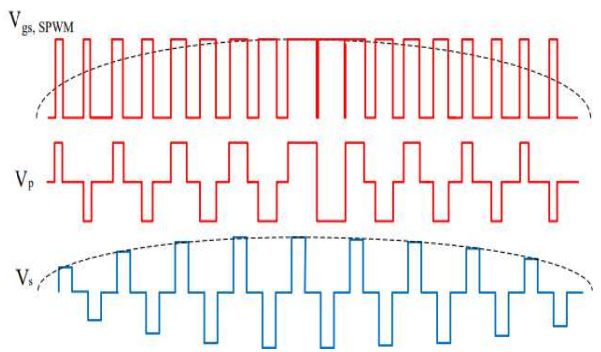


Fig. 3. The modulation waveforms of the DABR for AC output [13].

TABLE I. CONVERTER PARAMETERS

Parameters	Value
Power, P_o	1 kW
Port-1 voltage, V_I	200 V
Port-2 voltage, V ₂	200 V
Port-3 voltage, V_3	260 V
Resonant inductor, L_I	40 μΗ
Resonant inductor, L_2	40 μΗ
Resonant capacitor, C_I	0.047 μF
Resonant capacitor, C_2	0.047 μF
Phase shift, δ	108°
Phase shift, D_I	144°
Phase shift, D_2	144°
Turns ratio, N	2
Switching frequency, f_s	100 kHz

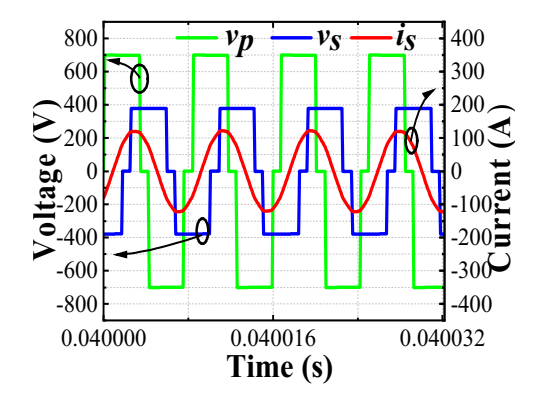


Fig. 4. Plot of v_p , v_s , i_s vs. time (s) for four cycles.

simplifies the implementation of the modulation scheme. However, it's important to note that over the course of a half cycle, multiple distinct fundamental TPS schemes are utilized. The gate pulses $V_{gs,SPWM}$ are responsible for controlling the switches in the primary bridge, resulting in the generation of the primary voltage denoted as V_P [13].

III. RESULTS

The proposed converter has been simulated in Matlab/Simulink. In addition to the simulation, a 1 kW prototype has been built to verify the proposed converter. The circuit specifications of the hardware implementation are illustrated in Table I. The simulation results for this converter are shown in Fig. 4 represents the three-level voltage waveforms

in the primary and secondary resonant tank. Also, it is apparent that the current through the resonant tank is sinusoidal and therefore, conduction loss is reduced significantly. Fig. 5(a) validates the ZVS turn on of all the switches. During each time instant (i.e., $t_0 - t_7$), the current is either positive or negative that confirms the ZVS turn on. For example, at t_0 , S_1 is turned on and i_S is negative. Therefore, the current goes through the bodydiode of S_1 and drain-source voltage of S_1 is zero. The same explanation is applicable for other switches ($S_2 - S_8$) in other time instants ($t_1 - t_7$). As a consequence, the switching loss of the converter is reduced greatly.

The experimental results of the converter are demonstrated in Fig. 5(b) – Fig. 5(f). The voltage waveforms across the primary side and secondary side resonant tank including the

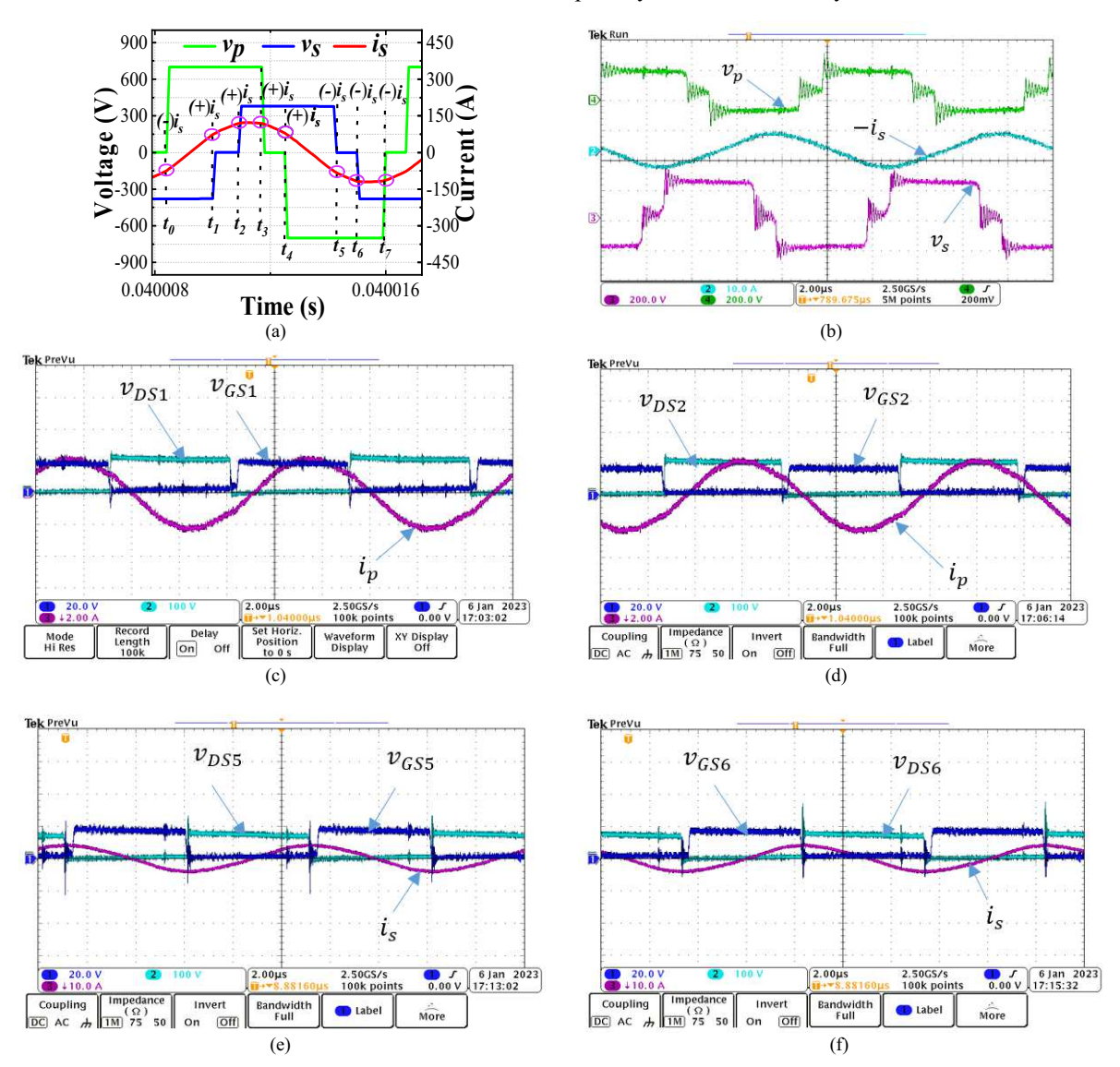


Fig. 5. (a) ZVS turn on verification based on the sign of i_s from time interval t_0 to t_7 . (b) Steady state waveforms v_p , v_s , $-i_s$ vs. time. (c) ZVS verification of switches: Switch S_2 drain-source voltage, gate source voltage and primary current. (d) ZVS verification of switches: Switch S_2 drain-source voltage, gate source voltage and secondary current. (f) Switch S_6 drain-source voltage, gate source voltage and secondary current.

resonant tank current are depicted in Fig. 5(b). The peak of voltage waveform in the primary resonant tank represents the input voltage V_1 and V_2 . The sinusoidal current waveform can be reshaped by varying the phase shifts (δ, D_1, D_2) . The ZVS turn on validation of the all the switches can be inferred from the sinusoidal current waveform. In addition, the drain to source voltage vs gate to source voltage of the switches are presented to verify the ZVS turn on of the switches. It is apparent from Fig. 5(c) – Fig. 5(f) that gate to source voltage starts increasing from zero voltage after drain to source voltage reaches zero. Therefore, ZVS turn on of the switch is confirmed.

By applying the modulation waveforms of the DABR for AC output, the AC voltage will appear in the output port, as shown in Fig. 6. The input DC voltage is configured at 48V, while the output voltage is adjusted to 155V peak (equivalent to 120V RMS) to align with the standard single-phase grid voltage.

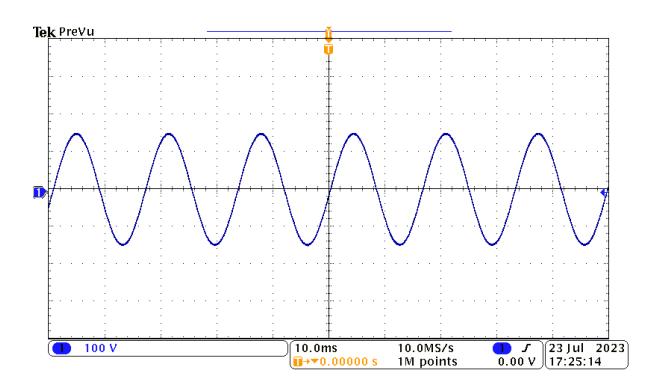


Fig. 6. The AC output voltage of the DABR.

IV. CONCLUSION

This paper presents a 1kW three-port converter based on dual active bridge resonant topology. The converter can integrate two input sources and provide dc or ac output depending on the modulation scheme. The operating principle of the converter has been discussed and the power flow equation has been derived. The proper design and adopted TPS modulation can secure ZVS turn on of all the switches. Both simulation and experiment were carried out to validate the operation of the converter. The results demonstrate that the converter can manage power flow between input and output with reduced conduction and switching loss.

ACKNOWLEDGMENT

This work is partially supported by NSF grant: NSF ECCS-2103442.

REFERENCES

- [1] U.S. Solar Market Insight, Solar Energy Industries Association. [Online]. Available: https://www.seia.org/us-solar-market-insight
- [2] M. Safayatullah, R. Rezaii, M.T. Elrais, and I. Batarseh, "Review of Control Methods in Grid-Connected PV and Energy Storage System," in IEEE 2021 Energy Conversion Congress and Expo, 2021, pp. 951-958.
- [3] A.K. Bhattacharjee, N. Kutkut, and I. Batarseh, "Review of Multiport Converters for Solar and Energy Storage Integration," *IEEE Trans. Power Electron.*, Vol. 34, no. 2, pp. 1431-1445, Feb. 2019.
- [4] R. Rezaii, S. Ghosh, M. Safayatullah, S. Milad Tayebi and I. Batarseh, "Quad-Input Single-Resonant Tank LLC Converter for PV Applications," *IEEE Trans. Industry Appl.*, vol. 59, no. 3, pp. 3438-3457, May-June 2023.
- [5] M. T. Elrais, M. Safayatullah and I. Batarseh, "Generalized Architecture of a GaN-Based Modular Multiport Multilevel Flying Capacitor Converter," *IEEE Trans. Power Electron.*, vol. 38, no. 8, pp. 9818-9838, Aug. 2023.
- [6] M. Safayatullah, M.T. Elrais, S. Ghosh, R. Rezaii, and I. Batarseh, "A Comprehensive Review of Power Converter Topologies and Control Methods for Electric Vehicle Fast Charging Applications," *IEEE Access.*, Vol. 10, pp. 40753-40793, Apr. 2022.
- [7] M. Salehi and M. Amirabadi, "A Soft-Switching Zeta-Based AC-Link Universal Converter," 2023 IEEE Applied Power Electronics Conference and Exposition (APEC), Orlando, FL, USA, 2023, pp. 3233-3239, doi: 10.1109/APEC43580.2023.10131175.
- [8] R. Rezaii et al., "Design and Implementation of a Multiport System for Solar EV Applications," 2023 IEEE Applied Power Electronics Conference and Exposition (APEC), Orlando, FL, USA, 2023, pp. 29-34, doi: 10.1109/APEC43580.2023.10131342.
- [9] M. Safayatullah and I. Batarseh, "Small Signal Model of Dual Active Bridge Converter for Multi-Phase Shift Modulation," in IEEE 2020 Energy Conversion Congress and Expo, 2020, pp. 5960-5965.
- [10] M. Safayatullah, R. Rezaii, F. Alaq and I. Batarseh, "A Three-Port DC-DC-DC Converter based on Dual Active Bridge Series Resonant Topology for Electric Vehicle DC Fast Charging Applications," in IEEE 2022 Energy Conversion Congress and Exposition (ECCE), 2022, pp. 1-7.
- [11] A. Zare, S. D'Silva, M. F. Umar and M. B. Shadmand, "Smart Battery Cells for Maximum Utilization in Power Electronics Dominated Grids," 2022 3rd International Conference on Smart Grid and Renewable Energy (SGRE), Doha, Qatar, 2022, pp. 1-6, doi: 10.1109/SGRE53517.2022.9774203.
- [12] A. Bhattacharjee and I. Batarseh, "An Interleaved Boost and Dual Active Bridge Based Three Port Microinverter," 2020 IEEE Applied Power Electronics Conference and Exposition (APEC), New Orleans, LA, USA, 2020, pp. 1320-1326, doi: 10.1109/APEC39645.2020.9124515.
- [13] A. Bhattacharjee and I. Batarseh, "A New Bidirectional AC-link Microinverter Based On Dual Active Bridge Topology," 2019 IEEE Applied Power Electronics Conference and Exposition (APEC), Anaheim, CA, USA, 2019, pp. 2268-2273, doi: 10.1109/APEC.2019.8722105.
- [14] R. W. A. A. De Doncker, D. M. Divan and M. H. Kheraluwala, "A three-phase soft-switched high-power-density DC/DC converter for high-power applications," *IEEE Trans. Industry. Appl.*, Vol. 27, no. 1, pp. 63-73, Jan. 1991.
- [15] M. Yaqoob, K. H. Loo and Y. M. Lai, "A Four-Degrees-of-Freedom Modulation Strategy for Dual-Active-Bridge Series-Resonant Converter Designed for Total Loss Minimization," *IEEE Trans. Power Electron.*, Vol. 34, no. 2, pp. 1065-1081, Feb. 2019.
- [16] H. Qin and J. W. Kimball, "Generalized Average Modeling of Dual Active Bridge DC-DC Converter," *IEEE Trans. Power Electron.*, Vol. 27, no. 4, pp. 2078-2084, Apr. 2012.